Colloid Polym Sci 280: 71–77 (2002)

ORIGINAL CONTRIBUTION

K. Sekine
C. Kuroda
N. Torii

Boundary-element calculations for dielectric relaxation of water-in-oil-in-water emulsions consisting of spherical droplets with a spheroidal core

Received: 8 May 2001
Accepted: 29 August 2001

K. Sekine (✉) · C. Kuroda · N. Torii
School of Health Sciences
Faculty of Medicine
Kanazawa University
5-11-80 Kodatsuno
Kanazawa 920-0942, Japan
e-mail: sekine@kenroku.kanazawa-u.ac.jp
Tel.: +81-76-2652586
Fax: +81-76-2344360

Abstract Using the boundary-element method, theoretical calculations were made for the complex permittivity of water-in-oil-in-water emulsions consisting of spherical droplets. A spheroidal inner phase was placed at the center of the droplet. To examine the effects of the shape of the inner phase, the axial ratio of the inner phase was changed by keeping its volume unchanged. The results showed that the dielectric relaxation of the emulsions was markedly affected by the shape of the inner phase. As a detailed analysis, effects of external electric fields directed in the mirror plane and those along the rotation axis of the droplets were examined separately. This showed that the relaxation consisted of two kinds of relaxation terms. The first related to the structure of the droplet parallel to the external field and had similar character to the low-frequency relaxation of emulsions of shelled spheres. The second, found in restricted cases, related to the structure perpendicular to the external field, having character similar to the high-frequency relaxation for the shelled spheres.

Keywords Boundary element method · Dielectric relaxation · Interfacial polarization · Emulsion

Introduction

Several dispersed systems show dielectric relaxation due to interfacial polarization in the radio-frequency region [1–13]. Since the dielectric relaxation of this kind depends on electrical and structural properties of the systems, dielectric spectroscopic techniques serve as nondestructive and *in situ* methods for the analysis of the interior of the dispersed particles, such as aqueous droplets in frozen water-in-oil (w/o) emulsions [2], biological cells [6–11], ion-exchange resins [12], and microcapsules [13].

In conventional theories of the interfacial polarization for emulsions, models of dispersed particles are limited to layered confocal ellipsoids [14, 15] because of mathematical difficulties. Discrepancies between the structure of such simplified models and that of real droplets reduce the utility of dielectric spectroscopic techniques. Recent progress in theoretical studies [16–20] enabled us to make computer-assisted calculations of the dielectric relaxation using realistic models, to which it was difficult to apply conventional analytical methods. In the present study, the dielectric relaxation of water-in-oil-in-water (w/o/w) emulsions consisting of spherical droplets is calculated with a method [19] using the boundary-element method (BEM). The shape of the inner phase, which was restricted to spherical in conventional theories, is made spheroidal in the present study. Calculations using these models are situated at the first stage of a series of theoretical examinations about the effects of the internal structure of the droplets using nonconventional models, which will be extended to more complicated specimens in the future, such as flocs in flocculated w/o emulsions [21] and biological cells containing plural intracellular organelles [10]. These calculations are expected to provide guidelines for estimating the detailed structure of the droplets.

Models and method of calculation

Models

The models for the droplets in the w/o/w emulsions are shown in Fig. 1. The outer surface of the droplet is spherical and is represented by

$$x^2 + y^2 + z^2 = 1 \ . \tag{1}$$

The inner phase has a spheroidal surface given by

$$\frac{x^2 + y^2}{R_{ih}^2} + \frac{z^2}{R_{iz}^2} = 1 \ , \tag{2}$$

where R_{ih} and R_{iz} are the semiaxes of the spheroid. The inner phase for model S is spherical ($R_{ih} = R_{iz} = 0.7$). By forcing the volume to be constant, the inner phase is modified into oblate spheroids in models O1 ($R_{ih} = 0.88$) and O2 ($R_{ih} = 0.95$) and into prolate ones in models P1 ($R_{iz} = 0.88$) and P2 ($R_{iz} = 0.95$). The following values were adopted for relative permittivities ε and electrical conductivities κ of the phases: $\varepsilon_i = \varepsilon_a = 80$, $\kappa_i = \kappa_a = 1$ mS m^{-1}, $\varepsilon_s = 35$, $\kappa_s = 0$, where subscripts i, a, and s denote the inner phase, a dispersing medium, and the shell-phase, respectively. The values of κ_i and κ_a are typical of aqueous electrolyte solutions [22]. The value of ε_s is comparable to the relative permittivity of nitrobenzene [23].

Method of calculation

In a previous study [19], we developed a method of calculating the complex permittivity ε^* of emulsions with the BEM, where ε^* is represented by $\varepsilon^* = \varepsilon + \kappa/(i\omega\varepsilon_0)$, with ε, κ, an imaginary unit i, angular frequency ω represented by $\omega = 2\pi f$ in terms of frequency, f, and the permittivity of vacuum, ε_0. This method is an extension of the analytical methods using Maxwell–Wagner–Sillars-type mixture equations [14, 24, 25], consisting of the following three steps:

1. When a piece of the droplet is placed in a uniform external electric field $\mathbf{E}_0(E_{0x}, E_{0y}, E_{0z})$, a dipole moment $\mathbf{p}$ is induced. Values of the electric potential ϕ due to $\mathbf{p}$ are calculated by solving Laplace's equation numerically using the BEM. Details of the calculations are shown in the Appendix.
2. The values of ϕ at a distant point $\mathbf{r}(x, y, z)$ from the droplet, which is placed at the origin of the Cartesian coordinate system, is represented by

$$\phi = \frac{1}{4\pi\varepsilon_a^*\varepsilon_0 r^3}\mathbf{pr} \ , \tag{3}$$

where ε_a^* is the complex permittivity of the surrounding medium and $r = (x^2 + y^2 + z^2)^{1/2}$. The induced moment $\mathbf{p}$ is represented using a polarizability tensor α of the droplet as $\mathbf{p} = \alpha\mathbf{E}_0$. When the droplet has $D_{\infty h}$ symmetry, as adopted in the present study, α is the diagonal consisting of the polarizability components α_h in the mirror plane (xy-plane) and α_z along the rotation axis (z-axis). Hence Eq. (3) is modified to

$$\phi = \frac{1}{4\pi\varepsilon_a^*\varepsilon_0 r^3}\left[\alpha_h(xE_{0x} + yE_{0y}) + \alpha_z zE_{0z}\right] = \frac{V}{4\pi r^3}\left[\beta_h(xE_{0x} + yE_{0y}) + \beta_z zE_{0z}\right] \ , \tag{4}$$

where β_k (k = h, z) is the polarization coefficient defined by $\beta_k = \alpha_k/(V\varepsilon_a^*\varepsilon_0)$ using α_k, ε_a^*, and the volume of the droplet V. In this step, values of β_k are obtained from ϕ using Eq. (4).
3. Using a Maxwell–Wagner–Sillars-type mixture equation, a formula for the equivalent complex permittivity ε^* of the emulsion is derived from Eq. (4) as

$$\frac{\varepsilon^* - \varepsilon_a^*}{\varepsilon^* + 2\varepsilon_a^*} = \frac{P}{9}(2\beta_h + \beta_z) \ , \tag{5}$$

where P is the volume fraction of the emulsion. When $P \ll 1$, Eq. (5) becomes [26]

$$\varepsilon_D^* = \varepsilon_D + \kappa_D/(i\omega\varepsilon_0) \equiv (\varepsilon^* - \varepsilon_a^*)/P = 2\varepsilon_{Dh}^* + \varepsilon_{Dz}^* \ , \tag{6}$$

where

$$\varepsilon_{Dk}^* = \varepsilon_{Dk} + \kappa_{Dk}/(i\omega\varepsilon_0) \equiv \varepsilon_a\beta_k/3 \ (k = h,z) \ . \tag{7}$$

The approximate relations, Eqs. (6) and (7), were used in the present study.

The calculations were made at frequencies from 10 to 10^9 Hz. The calculations of ϕ in step 1 for models O1, O2, P1, and P2 were carried out using the BEM, in which the surfaces of the droplets were divided into isoparameteric elements consisting of ten nodes, with cubic shape functions [27] being used in each of the elements. Preliminary examinations showed that at least three significant figures were attained in the calculations of ε_D^* when the surfaces were divided into more than 288 elements. Analytical equations [28] were used in the calculations for model S since it has a structure of a concentric shelled sphere.

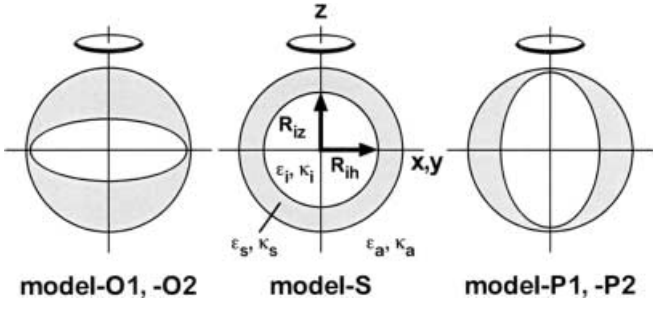

Fig. 1 Models for droplets in water-in-oil-in-water emulsions

Results and discussion

Behavior of β_k

The frequency dependence of β_k for model O2 is shown in Fig. 2. As seen from this figure, the behavior of β_k is dependent on the direction of the external field, $\mathbf{E}_0$; β_h shows two-step relaxation that includes two relaxation terms h1O and h2O at low and high frequencies, respectively, whereas β_z shows one-step relaxation z1O. Similar behavior of β_k was found for model-O1. In models P1 and P2, in contrast, β_h and β_z contained one (h1P) and two (z1P and z2P) relaxation terms, respectively. Since $R_{ih} = R_{iz}$ in model S, $\beta_h = \beta_z$, which contained two relaxation terms, 1S and 2S, at low and high frequencies, respectively.

Behavior of ε_{Dk}^*

The frequency-dependence of ε_{Dk}^* for model O2 is shown in Fig. 3. As seen from this figure, the behavior of ε_{Dk}^* is

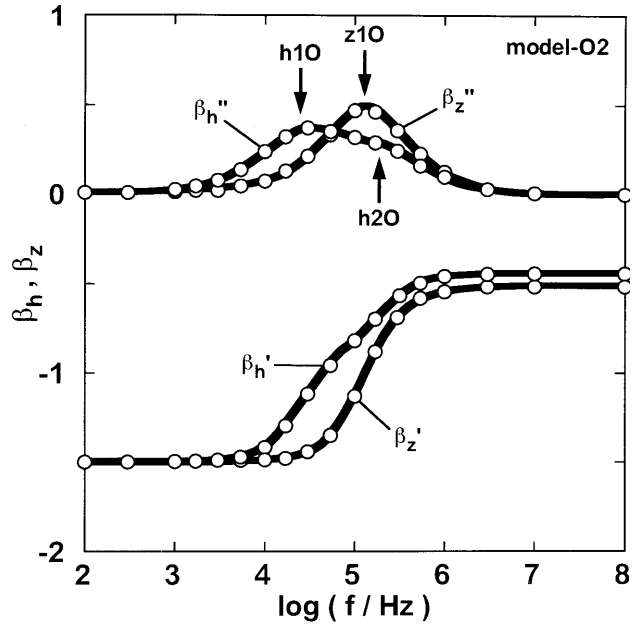

Fig. 2 Frequency-dependence of β_h ($=\beta_h' + i\beta_h''$) in the mirror plane and that of β_z ($=\beta_z' + i\beta_z''$) along the rotation axis for model O2

also dependent on the direction, because of the direction-dependent behavior of β_k. It is considered that the relaxation of ε_{Dk}* consists of the same relaxation terms as those in β_k. To obtain dielectric relaxation parameters for the terms in ε_{Dk}*, we assumed Cole–Cole-type relaxation [29] described by $D^e/[1 + (i\omega\tau^e_C)^{m^e_C}]$, where D^e is the relaxation intensity, τ^e_C the relaxation time, and m^e_C the Cole–Cole parameter. The characteristic frequency, $f^e_C = 1/(2\pi\tau^e_C)$, was obtained from τ^e_C. The same analysis was made for the other models. The values of these relaxation parameters are shown in Table 1.

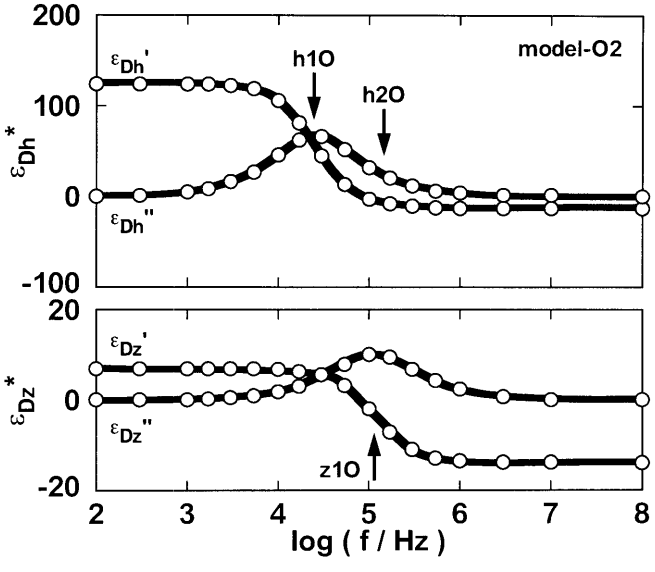

Fig. 3 Frequency-dependence of ε_{Dh}* [$=\varepsilon_{Dh}' - i\varepsilon_{Dh}'' + \kappa_{Dh}{}^L/(i\omega\varepsilon_0)$ where $\kappa_{Dh}{}^L$ is the limiting value of κ_{Dh} at low frequencies] in the mirror plane and ε_{Dz}* [$=\varepsilon_{Dz}' - i\varepsilon_{Dz}'' + \kappa_{Dz}{}^L/(i\omega\varepsilon_0)$] along the rotation axis for model O2

Table 1 Effects of the shape of the inner phase on the characteristic frequency f^e_C (kHz), the relaxation intensity D^e, and the Cole–Cole parameter m^e_C, for constituent relaxation terms in ε_{Dh}* and ε_{Dz}*

Model	O2	O1	S	P1	P2
T_h	0.050	0.120	0.300	0.376	0.399
T_z	0.620	0.557	0.300	0.120	0.050
Relaxation terms in ε_{Dh}*					
	h1O		*1S*	*h1P*	
f^e_C	25	41	74	84	85
D^e	134	78	39	34	34
m^e_C	1.00	1.00	1.00	1.00	0.99
	h2O		*2S*		
f^e_C	147	178	205		
D^e	2.64	1.55	0.74		
m^e_C	0.98	0.99	1.00		
Relaxation terms in ε_{Dz}*					
	z1O		*1S*	*z1P*	
f^e_C	114	110	74	46	32
D^e	21	23	39	69	98
m^e_C	0.99	1.00	1.00	1.00	1.00
			2S	*z2P*	
f^e_C			205	170	112
D^e			0.74	1.60	4.21
m^e_C			1.00	0.99	0.97

The direction-dependent behavior of β_k and ε_{Dk}* is considered to originate from the direction-dependent structure of the droplets. In the present study, further analysis of the behavior of ε_{Dk}* were carried out using the thickness of the shell phase in the mirror plane, $T_h = 1 - R_{ih}$, and that along the rotation axis, $T_z = 1 - R_{iz}$, as the measure of the structure of the droplets.

Plots of f^e_C and D^e of h1O, h2O, and h1P against T_h and those of z1O, z1P, and z2P against T_z are shown in Figs. 4 and 5. As a comparison with these relaxation terms, f^e_C and D^e of 1S and 2S for shelled spheres of model-S type were evaluated using the analytical equations [28] by changing the thickness T of the shell phase, and are represented by the solid lines in Figs. 4 and 5.

It is suggested from Figs. 4 and 5 that the relaxation terms in ε_{Dk}* can be classified into two types: type 1 including h1O, h1P, z1O, and z1P that have low f^e_C and large D^e, and type 2 including h2O and z2P having high f^e_C and small D^e. The behavior of type-1 relaxation terms is similar to that of 1S for the shelled spheres. The values of f^e_C and D^e of type-2 terms are located in the same regions as those of 2S; however the dependence of f^e_C and that of D^e on T are both opposite to those in 2S. As an attempt, f^e_C and D^e of

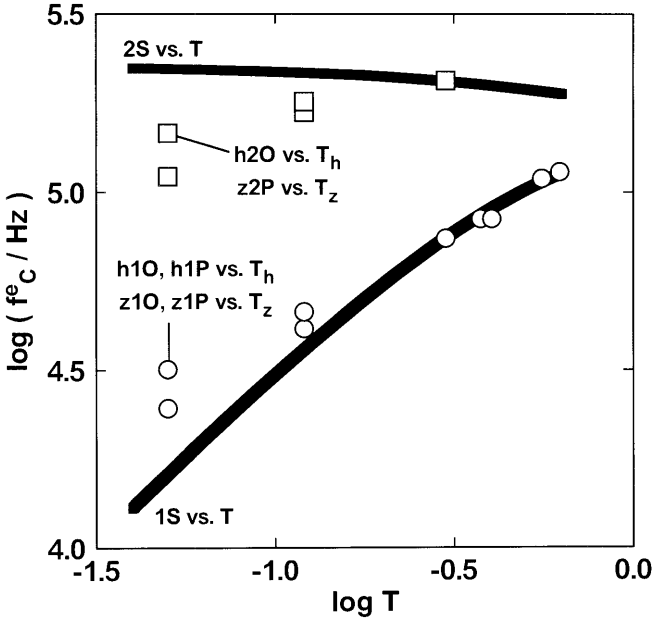

Fig. 4 Change in the characteristic frequency f^e_C of constituent relaxation terms with the thickness T of the shell phase parallel to an external electric field, $\mathbf{E}_0$

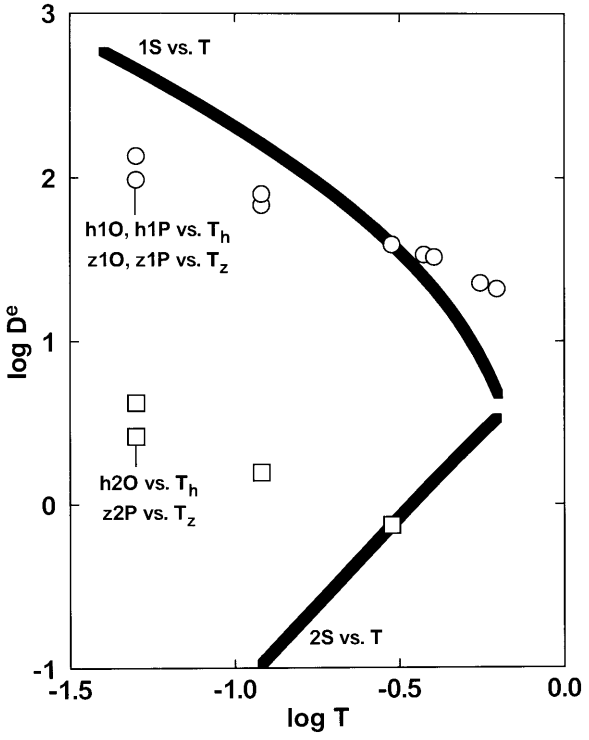

Fig. 5 Change in the relaxation intensity D^e of constituent relaxation terms with T parallel to $\mathbf{E}_0$

h2O are plotted against T_z, and those of z2P against T_h in Fig. 6, in which the behavior of type-2 relaxation terms is similar to 2S. This result indicates that h2O

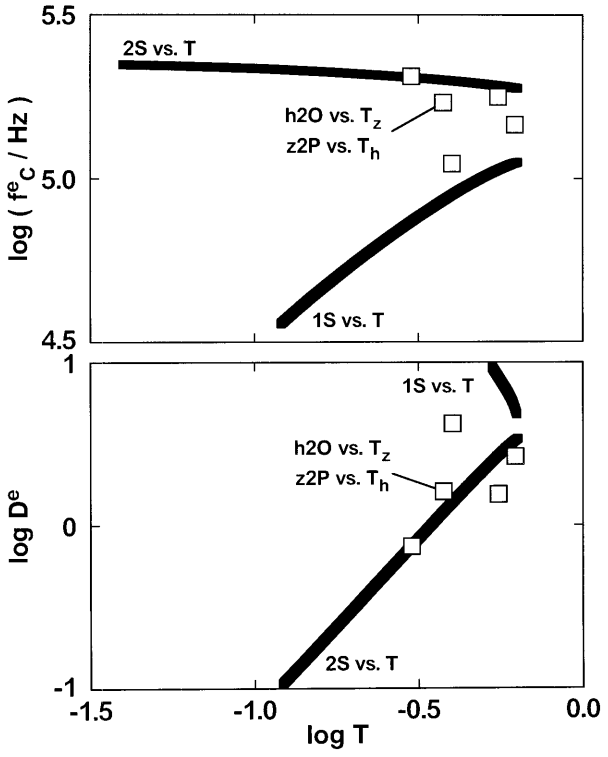

Fig. 6 Changes in f^e_C and D^e of h2O and z2P with T perpendicular to $\mathbf{E}_0$

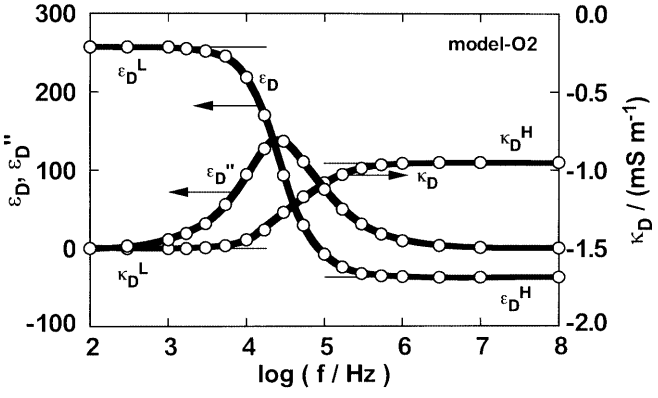

Fig. 7 Frequency dependence of ε_D^* $[=\varepsilon_D+\kappa_D/(i\omega\varepsilon_0)=\varepsilon_D'-i\varepsilon_D''+\kappa_D^L/(i\omega\varepsilon_0)]$ for model O2

and z2P are related to the structure of the droplet perpendicular to $\mathbf{E}_0$.

Behavior of ε_D^*

The frequency dependence of $\varepsilon_D^* = 2\varepsilon_{Dh}^* + \varepsilon_{Dz}^*$ for model O2 is shown in Fig. 7. The constituent relaxation terms h1O, h2O, and z1O are not distinguishable in this figure.

Table 2 Effects of shape of the inner phase on limiting values of the relative permittivity ε_D and the conductivity κ_D

Model	O2	O1	S	P1	P2
Low-frequency limit					
${\varepsilon_D}^L$	257	144	82	101	131
${\kappa_D}^L$/mS m^{-1}	−1.50	−1.50	−1.50	−1.50	−1.50
High-frequency limit					
${\varepsilon_D}^H$	−37.5	−37.8	−38.2	−38.1	−38.0
${\kappa_D}^H$/mS m^{-1}	−0.95	−0.97	−0.99	−0.98	−0.98

The limiting values ${\varepsilon_D}^L$, ${\varepsilon_D}^H$, ${\kappa_D}^L$, and ${\kappa_D}^H$ of ε_D and κ_D at low (L) and high (H) frequencies for the models used in the present study are shown in Table 2. It is clearly seen from this table that the shape of the inner phase causes effects on ε_D*, especially on ${\varepsilon_D}^L$. In models O1 and O2, the deformation of the inner phase causes a marked increase in D^e of h1O and a slight one of h2O, as seen from Table 1. The accompanying decrease in D^e of z1O is not serious. Hence the increase in ${\varepsilon_D}^L$ for these models is attributable to the increase in D^e of h1O. In a similar way, the increase in ${\varepsilon_D}^L$ for models P1 and P2 is attributable to that in D^e of z1P.

Conclusion

The present study showed that the dielectric relaxation of w/o/w emulsions is affected by the shape of the inner phase. This means that the utility of conventional confocal models is limited because the shape of the inner phase is restricted by that of the outer surface of the droplet in these models. It can be considered that the number and the position of the inner phases also affect the dielectric relaxation. Examinations of these effects using numerical methods will provide important information for developing detailed and reliable methods of analysis with dielectric spectroscopic techniques.

Acknowledgement The authors thank K. Asami, Institute for Chemical Research, Kyoto University, for helpful discussion.

Appendix

The induced electric potential, ϕ, around the droplet is obtained by solving Laplace's equation

$$\text{div grad } (\psi + \phi) = 0 \ , \tag{A1}$$

where ψ is the electric potential due to $\mathbf{E}_0$ ($=-$grad ψ). Using Green's theorem, $\psi + \phi_j$ at a point $P(x_p, y_p, z_p)$ on the surface of phase j (j = a, s, i) is represented by the surface integral equations as

$$c_a(P)[\psi(P) + \phi_a(P)] = \int_{\Gamma_\infty + \Gamma_o} [u^* q_a - q_a^*(\psi + \phi_a)] \mathrm{d}s \ , \tag{A2}$$

$$c_s(P)[\psi(P) + \phi_s(P)] = \int_{\Gamma_o + \Gamma_i} [u^* q_s - q_s^*(\psi + \psi_s)] \mathrm{d}s \ , \tag{A3}$$

$$c_i(P)[\psi(P) + \phi_i(P)] = \int_{\Gamma_i} [u^* q_i - q_i^*(\psi + \phi_i)] \mathrm{d}s \ , \tag{A4}$$

where Γ_∞ is the boundary at infinitely large distances from the droplet, Γ_o and Γ_i the surfaces represented by Eqs. (1) and (2), respectively, cj(P) the solid angle under which P sees the surfaces from phase j, u* the Green function

$$u^* = u^*(\mathbf{r}_p, \mathbf{r}) = \frac{1}{4\pi[(x - x_p)^2 + (y - y_p)^2 + (z - z_p)^2]^{1/2}} \ , \tag{A5}$$

$$q_j^* = (\text{grad } u^*)\mathbf{n}_j \ , \tag{A6}$$

$$q_j = [\text{grad } (\psi + \phi_j)]\mathbf{n}_j \ , \tag{A7}$$

and $\mathbf{n}_j$ the unit vector normal to the surface directed outside of phase j. Since $\phi = 0$ at infinitely large distances from the droplet, q_a and ϕ_a diminish on Γ_∞. Hence Eq. (A2) is reduced to

$$c_a(P)[\psi(P) + \phi_a(P)] = \psi(P) + \int_{\Gamma_o} [u^* q_a - q_a^*(\psi + \phi_a)] \mathrm{d}s \, . \tag{A8}$$

Using isoparameteric elements, Eqs. (A3), (A4), and (A8) are discretized into

$$\mathbf{H}_a^{\bar{o}\bar{o}} \boldsymbol{\phi}_a^o - \mathbf{G}^{\bar{o}\bar{o}} \mathbf{q}_a^o = (\mathbf{I} - \mathbf{H}_a^{\bar{o}\bar{o}}) \boldsymbol{\psi}^o \ , \tag{A9}$$

$$(\mathbf{H}_s^{\bar{o}\bar{o}} \boldsymbol{\phi}_s^o - \mathbf{G}^{\bar{o}\bar{o}} \mathbf{q}_s^o) + (\mathbf{H}_s^{oi} \boldsymbol{\phi}_s^i - \mathbf{G}^{oi} \mathbf{q}_s^i) = -(\mathbf{H}_s^{\bar{o}\bar{o}} \boldsymbol{\psi}^o + \mathbf{H}_s^{oi} \boldsymbol{\psi}^i) \ , \tag{A10}$$

$$(\mathbf{H}_s^{i\bar{o}} \boldsymbol{\phi}_s^o - \mathbf{G}^{io} \mathbf{q}_s^o) + (\mathbf{H}_s^{ii} \boldsymbol{\phi}_s^i - \mathbf{G}^{ii} \mathbf{q}_s^i) = -(\mathbf{H}_s^{io} \boldsymbol{\psi}^o + \mathbf{H}_s^{ii} \boldsymbol{\psi}^i) \ , \tag{A11}$$

$$\mathbf{H}_i^{ii} \boldsymbol{\phi}_i^i - \mathbf{G}^{ii} \mathbf{q}_i^i = -\mathbf{H}_i^{ii} \boldsymbol{\psi}^i \ , \tag{A12}$$

where

$$\boldsymbol{\psi}^m = {}^T\{\psi^M\} \ , \tag{A13}$$

$$\boldsymbol{\phi}_j^m = {}^T\{\phi_j^M\} \ , \tag{A14}$$

$$\mathbf{q}_j^m = {}^T\{\mathbf{q}_j^M\} \ , \tag{A15}$$

$$\mathbf{H}_{\mathrm{j}}^{\mathrm{mn}} = \{H_{\mathrm{j}}^{\mathrm{MN}}\} \ , \tag{A16}$$

$$\mathbf{G}^{\mathrm{mn}} = \{G^{\mathrm{MN}}\} \ , \tag{A17}$$

$$H_{\mathrm{j}}^{\mathrm{MN}} = \delta_{\mathrm{MN}} c_{\mathrm{j}}^{\mathrm{M}} + \int_{\Gamma_{\mathrm{n}}} [q_{\mathrm{j}}^{*}(\mathbf{r}_{\mathrm{M}}, \mathbf{r}) (N_{\mathrm{N}}(\mathbf{r})] \mathrm{d}s \ , \tag{A18}$$

$$G^{\mathrm{MN}} = \int_{\Gamma_{\mathrm{n}}} [u^{*}(\mathbf{r}_{\mathrm{M}}, \mathbf{r}) N_{\mathrm{N}}(\mathbf{r})] \mathrm{d}s \ , \tag{A19}$$

$$c_{\mathrm{j}}^{\mathrm{M}} = c_{\mathrm{j}}(P_{\mathrm{M}}) \ , \tag{A20}$$

I is the unit matrix, superscripts m and n index the surfaces Γ_{m} and Γ_{n} (m, n = i, o), M and N, respectively, index the nodes on Γ_{m} and Γ_{n}, $N_{\mathrm{N}}(\mathbf{r})$ is the shape function with respect to node N, and δ_{MN} is the Kronecker delta.

The following boundary conditions can be assumed at the surfaces Γ_{o} and Γ_{i}:

$$\phi_{\mathrm{j1}}^{\mathrm{M}} = \phi_{\mathrm{j2}}^{\mathrm{M}} \ , \tag{A21}$$

$$\varepsilon_{\mathrm{j1}}^{*} q_{\mathrm{j1}}^{\mathrm{M}} + \varepsilon_{\mathrm{j2}}^{*} q_{\mathrm{j2}}^{\mathrm{M}} = 0 \ , \tag{A22}$$

where (j1, j2) = (a, s) or (s, i). According to the definitions of $c_{\mathrm{j}}(P)$ and $q_{\mathrm{j}*}$,

$$c_{\mathrm{j1}}^{\mathrm{M}} + c_{\mathrm{j2}}^{\mathrm{M}} = 1 \ , \tag{A23}$$

$$q_{\mathrm{j1}}^{*}(\mathbf{r}_{\mathrm{M}}, \mathbf{r}) = -q_{\mathrm{j2}}^{*}(\mathbf{r}_{\mathrm{M}}, \mathbf{r}) \ . \tag{A24}$$

Using Eqs. (A21), (A22), (A23), and (A24) Eqs. (A9) and (A12) are, respectively, modified to

$$(\mathbf{I} - \mathbf{H}_{\mathrm{s}}^{\bar{\mathrm{o}}\bar{\mathrm{o}}}) \boldsymbol{\phi}_{\mathrm{s}}^{\mathrm{o}} + (\varepsilon_{\mathrm{s}}^{*}/\varepsilon_{\mathrm{a}}^{*}) \mathbf{G}^{\bar{\mathrm{o}}\bar{\mathrm{o}}} \mathbf{q}_{\mathrm{s}}^{\mathrm{o}} = \mathbf{H}_{\mathrm{s}}^{\bar{\mathrm{o}}\bar{\mathrm{o}}} \boldsymbol{\psi}^{\mathrm{o}} \ , \tag{A25}$$

$$(\mathbf{I} - \mathbf{H}_{\mathrm{s}}^{\mathrm{ii}}) \boldsymbol{\phi}_{\mathrm{s}}^{\mathrm{i}} + (\varepsilon_{\mathrm{s}}^{*}/\varepsilon_{\mathrm{i}}^{*}) \mathbf{G}^{\mathrm{ii}} \mathbf{q}_{\mathrm{s}}^{\mathrm{i}} = -(\mathbf{I} - \mathbf{H}_{\mathrm{s}}^{\mathrm{ii}}) \boldsymbol{\psi}^{i} \ , \tag{A26}$$

From Eqs. (A10), (A11), (A25), and (A26), we obtain

$$\begin{bmatrix} \mathbf{I} - \mathbf{H}_{\mathrm{s}}^{\bar{\mathrm{o}}\bar{\mathrm{o}}} & (\varepsilon_{\mathrm{s}}^{*}/\varepsilon_{\mathrm{a}}^{*}) \mathbf{G}^{\bar{\mathrm{o}}\bar{\mathrm{o}}} & \mathbf{0} & \mathbf{0} \\ \mathbf{H}_{\mathrm{s}}^{\bar{\mathrm{o}}\bar{\mathrm{o}}} & -\mathbf{G}^{\bar{\mathrm{o}}\bar{\mathrm{o}}} & \mathbf{H}_{\mathrm{s}}^{\mathrm{oi}} & -\mathbf{G}^{\mathrm{oi}} \\ \mathbf{H}_{\mathrm{s}}^{\mathrm{io}} & -\mathbf{G}^{\mathrm{io}} & \mathbf{H}_{\mathrm{s}}^{\mathrm{ii}} & -\mathbf{G}^{\mathrm{ii}} \\ \mathbf{0} & \mathbf{0} & \mathbf{I} - \mathbf{H}_{\mathrm{s}}^{\mathrm{ii}} & (\varepsilon_{\mathrm{s}}^{*}/\varepsilon_{\mathrm{i}}^{*}) \mathbf{G}^{\mathrm{ii}} \end{bmatrix} \begin{bmatrix} \boldsymbol{\phi}_{\mathrm{s}}^{\mathrm{o}} \\ \mathbf{q}_{\mathrm{s}}^{\mathrm{o}} \\ \boldsymbol{\phi}_{\mathrm{s}}^{\mathrm{i}} \\ \boldsymbol{\phi}_{\mathrm{s}}^{\mathrm{i}} \end{bmatrix} = - \begin{bmatrix} -\mathbf{H}_{\mathrm{s}}^{\bar{\mathrm{o}}\bar{\mathrm{o}}} & \mathbf{0} \\ \mathbf{H}_{\mathrm{s}}^{\bar{\mathrm{o}}\bar{\mathrm{o}}} & \mathbf{H}_{\mathrm{s}}^{\mathrm{oi}} \\ \mathbf{H}_{\mathrm{s}}^{\mathrm{io}} & \mathbf{H}_{\mathrm{s}}^{\mathrm{ii}} \\ \mathbf{0} & \mathbf{I} - \mathbf{H}_{\mathrm{s}}^{\mathrm{ii}} \end{bmatrix} \begin{bmatrix} \boldsymbol{\psi}^{\mathrm{o}} \\ \boldsymbol{\psi}^{\mathrm{i}} \\ \end{bmatrix} \ . \tag{A27}$$

This equation is used to evaluate $\boldsymbol{\phi}_{\mathrm{s}}^{\mathrm{o}}$, $\mathbf{q}_{\mathrm{s}}^{\mathrm{o}}$, $\boldsymbol{\phi}_{\mathrm{s}}^{\mathrm{i}}$, and $\mathbf{q}_{\mathrm{s}}^{\mathrm{i}}$ on the surfaces Γ_{o} and Γ_{i}, where $\boldsymbol{\psi}^{\mathrm{o}}$ and $\boldsymbol{\psi}^{\mathrm{i}}$ are given as boundary conditions characterizing $\mathbf{E}_0$.

If the point P is located outside the droplet, $c_{\mathrm{a}}(P) = 1$ in Eq. (A8); hence, Eq. (A8) becomes

$$\phi_{\mathrm{a}}(P) = \int_{\Gamma_{\mathrm{o}}} [u^{*} q_{\mathrm{a}} - q_{\mathrm{a}}^{*} (\psi + \phi_{\mathrm{a}})] \mathrm{d}s \ , \tag{A28}$$

which is discretized into

$$\begin{aligned} \boldsymbol{\phi}_{\mathrm{a}}(P) &= \mathbf{g}\mathbf{q}_{\mathrm{a}}^{\mathrm{o}} - \mathbf{h}_{\mathrm{s}}(\boldsymbol{\psi}^{\mathrm{o}} - \boldsymbol{\phi}_{\mathrm{a}}^{\mathrm{o}}) \\ &= -[(\varepsilon_{\mathrm{s}}^{*}/\varepsilon_{\mathrm{a}}^{*}) \mathbf{g}\mathbf{q}_{\mathrm{s}}^{\mathrm{o}} + \mathbf{h}_{\mathrm{a}}(\boldsymbol{\psi}^{\mathrm{o}} - \boldsymbol{\phi}_{\mathrm{s}}^{\mathrm{o}})] \ , \end{aligned} \tag{A29}$$

where

$$\mathbf{g} = {}^{\mathbf{T}}\{\mathrm{g}^{\mathrm{K}}\} \ , \tag{A30}$$

$$\mathbf{H}_{\mathrm{a}} = {}^{\mathrm{T}}\{h_{\mathrm{a}}^{\mathrm{K}}\} \ , \tag{A31}$$

$$\mathrm{g}^{\mathrm{K}} = \int_{\Gamma_{\mathrm{o}}} [u^{*}(\mathbf{r}_{P}, \mathbf{r}) N_{\mathrm{K}}(\mathbf{r})] \mathrm{d}s \ , \tag{A32}$$

$$h_{\mathrm{a}}^{\mathrm{K}} = \int_{\Gamma_{\mathrm{o}}} [q_{\mathrm{a}}^{*}(\mathbf{r}_{P}, \mathbf{r}) N_{\mathrm{K}}(\mathbf{r})] \mathrm{d}s \ . \tag{A33}$$

Equation (A29) is used to evaluated ϕ_{a} around the droplet using the values of $\boldsymbol{\phi}_{\mathrm{s}}^{\mathrm{o}}$ and $\mathbf{q}_{\mathrm{s}}^{\mathrm{o}}$.

References

1. Hanai T (1968) In: Sherman P (ed) Emulsion science. Academic, London, pp 353–478
2. Clausse M (1983) In: Becher P (ed) Encyclopedia of emulsion technology, vol 1. Dekker, New York, pp 481–715
3. Pethig R, Kell DB (1987) Phys Med Biol 32:933–970
4. Takashima S (1989) Electrical properties of biopolymers and membranes. Hilger, Bristol
5. Sjöblom J, Gestblom B (1992) In: Friberg SE, Lindman B (eds) Organized solutions. Dekker, New York, pp 193–219
6. Asami K (1998) In: Hackley VA, Texter J (eds) Handbook on ultrasonic and dielectric characterization techniques for suspended particulates. American Ceramic Society, Westerville, pp 333–349
7. Irimajiri A, Doida Y, Hanai T, Inouye A (1978) J Membr Biol 38:209–232
8. Irimajiri A, Hanai T, Inouye A (1979) J Theor Biol 78:251–269
9. Asami K, Irimajiri A (1984) Biochim Biophys Acta 778:570–578
10. Asami K, Yamaguchi T (1992) Biophys J 63:1493–1499
11. Higashiyama K, Sugimoto T, Yonezawa T, Fujikawa S, Asami K (1999) Biotechnol Bioeng 65:537–541
12. Ishikawa A, Hanai T, Koizumi N (1984) Bull Inst Chem Res Kyoto Univ 62:251–285
13. Sekine K, Zhang H, Hanai T (1991) Bull Inst Chem Res Kyoto Univ 69:450–458
14. Pauly H, Schwan HP (1959) Z Naturforschg B 14:125–131
15. Stepin LD (1965) Sov Phys Tech Phys 10:768–772
16. Vrinceanu D, Gheorghiu E (1996) Bioelectrochem Bioenerg 40:167–170

17. Clauzon P, Krähenbühl L, Nicolas A (1999) IEEE Trans Magn 35:1223–1226
18. Brosseau C, Beroual A (1999) Eur Phys J Appl Phys 6:23–31
19. Sekine K (2000) Bioelectrochem 52:1–7
20. Lei J, Wan JTK, Yu KW, Sun H (2001) J Phys Condens Matter 13:3583–3589
21. Skodvin T, Sjöblom J (1996) J Colloid Interface Sci 182:190–198
22. Vanýsek P (1998) In: Lide DR (ed) CRC handbook of chemistry and physics. CRC, Boca Raton, p 5:92
23. Laboratory for Insulation Research, Massachusetts Institute of Technology (1995) In: von Hippel A (ed) Dielectric materials and applications, 2nd edn. Artech House, Boston, pp 291–433
24. Wagner KW (1914) Arch Electrotech 2:371–387
25. Sillars RW (1936) J Inst Electr Eng 80:378–394
26. Asami K, Yonezawa T (1995) Biochim Biophys Acta 1245:317–324
27. Lean MH, Friedman M, Wexler A (1979) In: Banerjee PK, Butterfield R (eds) Developments in boundary element methods, vol 1. Elsevier, NewYork, pp 207–250
28. Asami K, Hanai T, Koizumi N (1980) Jpn J Appl Phys 19:359–365
29. Cole KS, Cole RH (1941) J Chem Phys 9:341–351